Control Engineering Practice 85 (2019) 23–33

Contents lists available at ScienceDirect

Control Engineering Practice

journal homepage: www.elsevier.com/locate/conengprac

Force, orientation and position control in redundant manipulators in prioritized scheme with null space compliance

Abbas Karami [a], Hamid Sadeghian [b,*], Mehid Keshmiri [a], Giuseppe Oriolo [c]

[a] Mechanical Engineering Department, Isfahan University of Technology, Isfahan, Iran
[b] Engineering Department, University of Isfahan, Isfahan, Iran
[c] Dipartimento di Ingegneria Informatica, Automatica e Gestionale, Sapienza Università di Roma, Rome, Italy

ARTICLE INFO

Keywords:
Force control
Orientation control
Prioritized control
Disturbance observer
Null space compliance

ABSTRACT

This paper addresses the problem of executing multiple prioritized tasks for robot manipulators with compliant behavior in the remaining null space. A novel controller–observer is proposed to ensure accurate accomplishment of various tasks based on a predefined hierarchy using a new priority assignment approach. Force control, position control and orientation control are considered. Moreover, a compliant behavior is imposed in the null space to handle physical interaction without using joint torque measurements. Asymptotic stability of the task space error and external torque estimation error during executing multiple tasks are shown. The performance of the proposed approach is evaluated on a 7R light weight robot arm by several case studies.

1. Introduction

Robots are termed kinematically redundant when they possess more degrees of freedom (DOF) than those necessary to achieve the desired task. Redundant robots have numerous significant advantages in comparison with non-redundant ones. In addition to classical applications of redundant DOF for singularity avoidance, performance optimization, *etc*., the possibility to define additional tasks besides the main task can also be provided. Both manipulators and humanoids robots can take this advantage to accomplish more complex tasks, effectively.

Nowadays it is essential for robots to be capable of executing various tasks in dynamic environments. Moreover, robots should ensure the safety of themselves and other entities such as a human in unknown and unpredictable places. These issues should be considered along with the accuracy of manipulation. Precise accomplishment of the tasks is critical to employ robots in delicate and vital tasks.

Task priority strategy has been developed for both first-order and second-order differential kinematics. In the prioritized control approaches, it is usual to project the Jacobian of the lower priority tasks to the null space of the higher priority tasks which ensures exact prioritization (Flacco, De Luca, & Khatib, 2012; Mistry, Nakanishi, & Schaal, 2007; Ott, Dietrich, & Albu-Schäffer, 2015; Park & Khatib, 2005; Sadeghian, Villani, Keshmiri, & Siciliano, 2013; Siciliano & Slotine, 1991). These methods are known as strict prioritization approach. The alternative methods for priority assignment are non-strict approaches. Non-strict priority allocation algorithms are usually handled by employing weighting methods which a lower priority task is not enforced to execute in the null space of higher priority tasks (see for example Bouyarmane & Kheddar, 2011 and Collette, Micaelli, Andriot, & Lemerle, 2007). Hence, the method does not guarantee to follow the imposed hierarchy, strictly. Recently, a method for smooth changing from a non-strict case to a strict one is suggested in Liu, Tan, and Padois (2016).

Velocity based task sequencing control with strict task priority is widely employed in different scenarios such as controlling the position of multiple points in Flacco and De Luca (2014) and visual servoing in Sadeghian, Villani, Kamranian, and Karami (2015) and De Luca, Ferri, Oriolo, and Giordano (2008). Task prioritization in acceleration level is more complex but improves the accuracy of the task execution. Prioritization method also affects the null space stability analysis. Stability analysis of the null space is critical in the acceleration level. The stability analysis of the internal motion during multi-priority acceleration level control was first performed in Hsu, Mauser, and Sastry (1989). The stability of this algorithm has been investigated in more details in Nakanishi, Cory, Mistry, Peters, and Schaal (2008) and Sadeghian et al. (2013). Torque level control is an alternative formulation which has been exploited both for humanoids (Khatib & Chung, 2014; Sentis, Park, & Khatib, 2010) and robotic arms (Ott et al., 2015).

Operational Space Formulation proposed in Khatib (1987) is the most common approach used for controlling the robot in the task space. Computing decoupled dynamics for the first task and designing the controller according to this dynamic constitute the basis of this formulation. In this way, handling multiple tasks is possible as it is performed

* Corresponding author.
E-mail addresses: a.karami@me.iut.ac.ir (A. Karami), h.sadeghian@eng.ui.ac.ir (H. Sadeghian), mehdik@cc.iut.ac.ir (M. Keshmiri), oriolo@diag.uniroma1.it (G. Oriolo).

https://doi.org/10.1016/j.conengprac.2019.01.003
Received 20 May 2018; Received in revised form 16 October 2018; Accepted 1 January 2019
Available online xxxx
0967-0661/© 2019 Elsevier Ltd. All rights reserved.

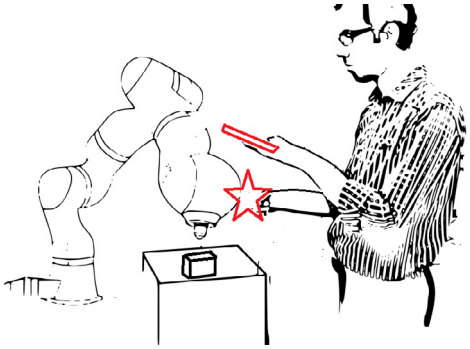

Fig. 1. Accidental interaction with robot working in social environment.

in Sentis et al. (2010). Complete stability analysis of both acceleration level and torque level approaches are performed in Sadeghian, Villani, Keshmiri, and Siciliano (2014) by the authors of this paper. Recently, a new formulation with specific null space velocity coordinates has been defined in Ott et al. (2015). This formulation is not intuitive but the resulted coordinates which are used for compliance control of prioritized tasks simplify the stability analysis of the system.

Force control has significant applications in surgical robots (Corteso & Dominici, 2017; Kesner & Howe, 2011; Navkar, Deng, Shah, Bekris, & Tsekos, 2012; Zemiti, Morel, Ortmaier, & Bonnet, 2007), industrial robots (Polverini et al., 2016; Winkler & Such, 2013) and humanoids (Khatib & Chung, 2014; Nicolis, Zanchettin, & Rocco, 2016; Sato et al., 2011). These applications include controlling interaction force between the robot and unknown soft or hard environments. The employed methods aim to extend the application of the robots for effective execution of the complex tasks. However, in all the researches force control is accomplished in the absence of accidental interactions that makes the control problem more elaborating. In the absence of tactile sensors on the robot body, observer is the most useful solution to estimate accidental interactions. Besides force control task, position and orientation control task in other directions should be usually considered (see for example Sato et al., 2011 and Jung, Hsia, & Bonitz, 2004). Orientation control is also a new field of interest especially in visual-servoing tasks (Khatib, Khudir, & De Luca, 2017). To the best of our knowledge, force and orientation control along with position control in task space and complaint behavior in null space have not been studied so far.

In this paper, the problem of handling external interactions with robot body during executing prioritized tasks is investigated. An example of the application scenario is depicted in Fig. 1, where robot works in collaboration with a human. External interaction on the robot must be considered in the control algorithm to perform the task successfully. Previously in Sadeghian et al. (2014), a position control task with null space compliance was considered. In this work, a novel method for defining coordinates of the hierarchical tasks is exploited (Section 3). The main purpose of this definition is to obtain an intuitive and integrated approach to prioritize multiple tasks besides introducing null space with minimal dimension. This is a critical issue to obtain the desired compliance behavior in the null space (see details in Sadeghian et al. (2013)).

The main contribution of this work is the proposing of a controller–observer algorithm to control force, position and orientation along with compliant behavior in the redundant degrees of freedom. Using external torque estimation algorithm, the execution of the prioritized tasks with minimum error is guaranteed during external interaction. Asymptotic stability of the overall system is proved in Section 4. The performance of the system which is evaluated experimentally on a 7DOF KUKA LWR arm is reported in Section 5.

Table 1
Nomenclature.

Variable	Description
$\boldsymbol{q}$	Robot joint configuration vector
t	Time
$\boldsymbol{M}(\boldsymbol{q})$	Robot inertia matrix in joint space
$\boldsymbol{C}(\boldsymbol{q},\dot{\boldsymbol{q}})$	Coriolis/centrifugal matrix in the joint space
$\boldsymbol{g}(\boldsymbol{q})$	Robot gravity vector in joint space
$\boldsymbol{\tau}$	Robot control torque in joint space
$\boldsymbol{J}(\boldsymbol{q})$	Robot Jacobian matrix
$\boldsymbol{J}_i(\boldsymbol{q})$	ith task Jacobian matrix
$\boldsymbol{J}_f(\boldsymbol{q})$	Physical contact Jacobian matrix
$\bar{\boldsymbol{J}}_i(\boldsymbol{q})$	New Jacobian of the ith task
$\boldsymbol{J}_{aug,i}(\boldsymbol{q})$	Augmentation of the new Jacobian matrices from 1 to i
$\boldsymbol{\tau}_{ext}$	External accidental torque
$\boldsymbol{\Lambda}_i(\boldsymbol{q})$	Inertia matrix in the ith task space
$\boldsymbol{\mu}_i(\boldsymbol{q},\dot{\boldsymbol{q}})$	Coriolis/centrifugal vector in the ith task space
$\boldsymbol{p}_i(\boldsymbol{q})$	Gravity vector in the ith task space
$\boldsymbol{f}_{control,i}$	Control command in ith task space
$\boldsymbol{f}_f$	Intentional contact force
$\boldsymbol{Z}_i(\boldsymbol{q})$	Null space based matrix for the ith task
$\boldsymbol{P}_i(\boldsymbol{q})$	Null space projector of for ith task
$\boldsymbol{x}$	Operational space coordinates for the ith task
$\bar{\boldsymbol{x}}$	New operational space coordination for the ith task
$\boldsymbol{\nu}$	Null space velocity coordinates
$\boldsymbol{p}(t)$	Linear momentum
$\boldsymbol{r}(t)$	Residual vector
$\boldsymbol{K}_{env}$	Environment stiffness
$\boldsymbol{C}_{env}$	Environment damping
$\boldsymbol{K}_{obs}$	Observer gain
$\boldsymbol{K}_{i,d}$	Derivative gain for the ith task space
$\boldsymbol{K}_{i,p}$	Proportional gain for the ith task space
$\boldsymbol{K}_{i,i}$	Integral gain for the ith task space
$\boldsymbol{R}_e$	Rotation matrix of the end effector
$\boldsymbol{\omega}_k^j$	Angular velocity of link "k" w.r.t frame "j"
$\boldsymbol{\eta}_k$	Scaler part of the quaternion representation of the orientation of the link "k"
$\boldsymbol{\epsilon}_k^j$	Vector part of quaternion representation of the orientation of the link "k" w.r.t frame "j"

2. Preliminaries

Herein, some critical and fundamental issues regarding this work will be reviewed. Since numerous parameters are defined and employed in this work, a nomenclature of the parameters is introduced in Table 1.

The dynamic model of a n-link robot with one physical contact point with the environment can be written as,

$$\boldsymbol{M}(\boldsymbol{q})\ddot{\boldsymbol{q}} + \boldsymbol{C}(\boldsymbol{q},\dot{\boldsymbol{q}})\dot{\boldsymbol{q}} + \boldsymbol{g}(\boldsymbol{q}) = \boldsymbol{\tau} - \boldsymbol{\tau}_{ext} - \boldsymbol{J}_f^T(\boldsymbol{q})\boldsymbol{f}_f, \tag{1}$$

where $\boldsymbol{M}(\boldsymbol{q}) \in \mathbb{R}^{n\times n}$ is the robot inertia matrix as a function of the joint configuration $\boldsymbol{q} \in \mathbb{R}^{n\times 1}$, $\boldsymbol{C}(\boldsymbol{q},\dot{\boldsymbol{q}})\dot{\boldsymbol{q}} \in \mathbb{R}^{n\times 1}$ represents Coriolis/centrifugal effects, and $\boldsymbol{g}(\boldsymbol{q}) \in \mathbb{R}^{n\times 1}$ is gravitational torques vector. Furthermore, $\boldsymbol{\tau} \in \mathbb{R}^{n\times 1}$ is the robot control torques and $\boldsymbol{\tau}_{ext} \in \mathbb{R}^{n\times 1}$ is the external torques resulting from external interactions with the environment. Moreover, $\boldsymbol{J}_f(\boldsymbol{q}) \in \mathbb{R}^{n_f\times n}$ is the Jacobian matrix of the force control task where n_f is the task dimension, and $\boldsymbol{f}_f$ is $(n_f \times 1)$ intentional contact force vector applied to the robot. In the case of multi-contact problem $\boldsymbol{J}_f^T(\boldsymbol{q})\boldsymbol{f}_f$ should be replaced with proper term including all the contact forces.

Considering l different tasks, the ith task coordinate vector $\boldsymbol{x}_i \in \mathbb{R}^{n_i}$ is related to the joint space vector through the mapping $\boldsymbol{x}_i = \boldsymbol{h}_i(\boldsymbol{q})$ for $1 \le i \le l$. Hence, the task space velocities $\dot{\boldsymbol{x}}_i$ are related to the joint space velocities $\dot{\boldsymbol{q}}$ by

$$\dot{\boldsymbol{x}}_i = \boldsymbol{J}_i(\boldsymbol{q})\dot{\boldsymbol{q}}, \tag{2}$$

where $\boldsymbol{J}_i(\boldsymbol{q}) = \frac{\partial \boldsymbol{h}_i}{\partial \boldsymbol{q}}$ is the Jacobian matrix of the ith task. In the case of position control tasks, following the operational space formulation introduced in Khatib (1987), the ith task space dynamics can be written as

$$\boldsymbol{\Lambda}_i(\boldsymbol{q})\ddot{\boldsymbol{x}}_i + \boldsymbol{\mu}_i + \boldsymbol{p}_i(\boldsymbol{q}) = \boldsymbol{f}_{control,i} - \boldsymbol{f}_f - \boldsymbol{J}_i^{\#T}(\boldsymbol{q})\boldsymbol{\tau}_{ext}, \tag{3}$$

where

$$\begin{aligned}&\boldsymbol{\Lambda}_i(\boldsymbol{q}) = (\boldsymbol{J}_i(\boldsymbol{q})\boldsymbol{M}^{-1}(\boldsymbol{q})\boldsymbol{J}_i^T(\boldsymbol{q}))^{-1},\\ &\boldsymbol{\mu}_i(\boldsymbol{q},\dot{\boldsymbol{q}}) = \boldsymbol{J}_i^{\#^T}(\boldsymbol{q})\boldsymbol{C}(\boldsymbol{q},\dot{\boldsymbol{q}})\dot{\boldsymbol{q}} - \boldsymbol{\Lambda}_i(\boldsymbol{q})\dot{\boldsymbol{J}}_i(\boldsymbol{q})\dot{\boldsymbol{q}},\\ &\boldsymbol{p}_i(\boldsymbol{q}) = \boldsymbol{J}_i^{\#^T}(\boldsymbol{q})\boldsymbol{g}(\boldsymbol{q}).\end{aligned} \tag{4}$$

$\boldsymbol{\Lambda}_i(\boldsymbol{q}) \in \mathbb{R}^{n_i\times n_i}$, $\boldsymbol{\mu}_i(\boldsymbol{q}) \in \mathbb{R}^{n_i\times n_i}$ and $\boldsymbol{p}_i(\boldsymbol{q}) \in \mathbb{R}^{n_i\times 1}$ are the inertia matrix, Coriolis/centrifugal vector and gravity vector in ith task space, respectively. $\boldsymbol{f}_{control,i}$ is a $(n_i \times 1)$ vector represents the ith task control command and $\boldsymbol{J}_i^{\#}(\boldsymbol{q}) \in \mathbb{R}^{n\times n_i}$ denotes the inertia weighted generalized inverse of the ith task Jacobian (Khatib, 1987). Control torques are related to the task control command through $\boldsymbol{\tau} = \Sigma_{i=1}^{i=l}\boldsymbol{J}_i^T(\boldsymbol{q})\boldsymbol{f}_{control,i}$. Using proper projected Jacobian along with the associated dynamically consistent generalized inverse ensures decoupled inertia matrix (Khatib, 1995; Park & Khatib, 2005) as[1]

$$\boldsymbol{\Lambda} = diag(\boldsymbol{\Lambda}_1, \boldsymbol{\Lambda}_2, \dots \boldsymbol{\Lambda}_l). \tag{5}$$

We are looking for a task prioritization scheme with the following specifications;

- Lower priority tasks do not disturb the higher ones. In other words, the jth task should not disturb the ith task where $j > i \geq 1$.
- The dimension of the lowest level of hierarchy should be obtained as $n_l = n - \sum_{i=1}^{l-1} n_i$. Thus, the null space dynamics is introduced with n_l independent coordinates.

3. Problem formulation

In order to obtain a prioritized scheme with aforementioned characteristics, a new set of coordinates is needed. The $(n_i \times n)$ matrix $\bar{\boldsymbol{J}}_i(\boldsymbol{q})$ is proposed as

$$\bar{\boldsymbol{J}}_i(\boldsymbol{q}) = \begin{cases}\boldsymbol{J}_1 & i = 1\\ \boldsymbol{J}_i\boldsymbol{Z}_{i-1}^T(\boldsymbol{Z}_{i-1}\boldsymbol{M}\boldsymbol{Z}_{i-1}^T)^{-1}\boldsymbol{Z}_{i-1}\boldsymbol{M} & i = 2,\dots,l-1\\ (\boldsymbol{Z}_{l-1}\boldsymbol{M}\boldsymbol{Z}_{l-1}^T)^{-1}\boldsymbol{Z}_{l-1}\boldsymbol{M} & i = l,\end{cases} \tag{6}$$

where $\boldsymbol{Z}_{i-1}(\boldsymbol{q}) \in \mathbb{R}^{n-\sum_{j=1}^{i-1} n_j\times n}$ spans the complete null space of all previous tasks with minimal necessary dimension. Constructing $\boldsymbol{Z}_{i-1}$ is not unique and special care must be taken for its computation. Singular value decomposition can be utilized to obtain null space base Jacobian $\boldsymbol{Z}_{i-1}$. However, the analytical method discussed in Ott (2008) is used to ensure matrix continuity. For this purpose, the augmented Jacobian matrix is constructed as,

$$\boldsymbol{J}_{aug,i} = \begin{bmatrix}\bar{\boldsymbol{J}}_1\\ \bar{\boldsymbol{J}}_2\\ \vdots\\ \bar{\boldsymbol{J}}_i\end{bmatrix}, \tag{7}$$

and the null space base matrices for computation of the Jacobian of the tasks $2,\dots,i$ are obtained such that,

$$\boldsymbol{J}_{aug,i}\boldsymbol{Z}_i^T = \boldsymbol{0}. \tag{8}$$

In (6), $\boldsymbol{Z}_{i-1}^T(\boldsymbol{Z}_{i-1}\boldsymbol{M}\boldsymbol{Z}_{i-1}^T)^{-1}\boldsymbol{Z}_{i-1}\boldsymbol{M}$ is the projection operator to the space where the rows of $\boldsymbol{Z}_{i-1}$ are its base vectors. Similar operator definition can be found for example in Ott (2008). To the best of our knowledge, until now it has not been employed for prioritization multiple tasks. By calling this projector as $\boldsymbol{T}_{i-1} \in \mathbb{R}^{n\times n}$, it is obvious that $\boldsymbol{T}_{i-1}$ is idempotent and also fulfills $\boldsymbol{T}_{i-1}\boldsymbol{Z}_{i-1}^T = \boldsymbol{Z}_{i-1}^T$. The dimension of $\bar{\boldsymbol{J}}_l$ is $(n - \sum_{i=1}^{l-1} n_i \times n)$ which is a significant feature to obtain the desired stable behavior in the null space of the higher priority tasks (for more details Nakanishi et al., 2008 and Sadeghian et al., 2013 are referred).

The kinematic relation between the joint and the task space velocities are then given as

$$\dot{\boldsymbol{x}} = \boldsymbol{J}_{aug,l}\dot{\boldsymbol{q}}. \tag{9}$$

[1] Variables dependency in $\boldsymbol{q}$ and $\dot{\boldsymbol{q}}$ are shown in the first usage of the variables and are omitted elsewhere for the sake of brevity.

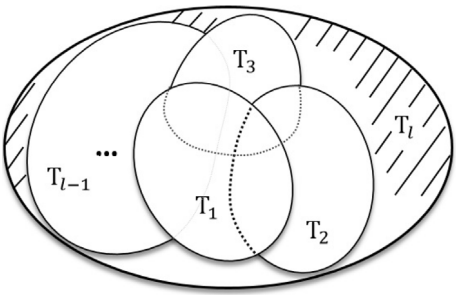

Fig. 2. Graphical interpretation of hypothetical prioritized tasks in the joint space. T_i shows the ith task and T_l (shaded) is the null space of all major tasks. While solid lines display the boundary of each task which is accessible in hierarchical scheme, dashed lines describe the omitted part of the task with respect to the priority allocation.

Denoting that by using (6), $\boldsymbol{J}_{aug,l}$ is $(n \times n)$ nonsingular matrix for full rank and independent $\boldsymbol{J}_i$. $\dot{\boldsymbol{x}}$ and $\dot{\boldsymbol{q}}$ are $(n\times 1)$ task and joint space velocity vectors. For given task velocity, the general solution for (9) can be written as

$$\dot{\boldsymbol{q}} = \boldsymbol{J}_{aug,l}^{-1}\dot{\tilde{\boldsymbol{x}}}, \tag{10}$$

where $\dot{\tilde{\boldsymbol{x}}} = \left[\dot{\boldsymbol{x}}_1, \dot{\boldsymbol{x}}_2, \dots, \dot{\boldsymbol{x}}_{l-1}, \boldsymbol{\nu}\right]^T$. $\boldsymbol{\nu}$ is $(n_l \times 1)$ null space velocity vector which is in general non-integrable (De Luca & Oriolo, 1997).

Dynamically consistent generalized inverse $\bar{\boldsymbol{J}}_i^{\#}$ is defined as

$$\bar{\boldsymbol{J}}_i^{\#} = \begin{cases}\boldsymbol{M}^{-1}\bar{\boldsymbol{J}}_i^T(\bar{\boldsymbol{J}}_i\boldsymbol{M}^{-1}\bar{\boldsymbol{J}}_i^T)^{-1} & i = 1,\dots,l-1,\\ \boldsymbol{Z}_{l-1}^T & i = l.\end{cases} \tag{11}$$

and by exploiting (7) and (8) along with (6) we have

$$\begin{cases}\boldsymbol{J}_1\boldsymbol{Z}_1^T = 0, & i = 1,\\ \boldsymbol{J}_j\boldsymbol{Z}_{j-1}^T(\boldsymbol{Z}_{j-1}\boldsymbol{M}\boldsymbol{Z}_{j-1}^T)^{-1}\boldsymbol{Z}_{j-1}\boldsymbol{M}\boldsymbol{Z}_i^T = 0, & i = 2,\dots,l,\end{cases} \tag{12}$$

for $j \leq i$. Recent relations can be exploited to ensure the fulfillment of

$$\boldsymbol{J}_{aug,i-1}\bar{\boldsymbol{J}}_i^{\#} = \boldsymbol{0}, \tag{13}$$

and

$$\bar{\boldsymbol{J}}_j\boldsymbol{M}^{-1}\bar{\boldsymbol{J}}_i^T = \boldsymbol{0} \qquad \text{for any } i \text{ and } j. \tag{14}$$

Eq. (13) guarantees the order of priority as shown in Fig. 2. Restriction of the lower priority tasks when they conflict with the higher priority tasks is demonstrated by using solid and dashed lines in Fig. 2. Moreover (14) ensures dynamical consistency and block diagonal inertia matrix (Ott et al., 2015). By observing (14), one can show

$$\boldsymbol{J}_{aug,l}^{-1} = \begin{bmatrix}\bar{\boldsymbol{J}}_1^{\#} & \bar{\boldsymbol{J}}_2^{\#} & \dots & \bar{\boldsymbol{J}}_l^{\#}\end{bmatrix}, \tag{15}$$

employing similar approach followed in Oh, Chung, and Youm (1998) and Sadeghian et al. (2013).

Eq. (10) can be extended to the second order kinematic solution as

$$\ddot{\boldsymbol{q}} = \boldsymbol{J}_{aug,l}^{-1}(\ddot{\tilde{\boldsymbol{x}}} - \dot{\boldsymbol{J}}_{aug,l}\dot{\boldsymbol{q}}), \tag{16}$$

where

$$\ddot{\tilde{\boldsymbol{x}}} = \begin{bmatrix}\ddot{\boldsymbol{x}}_1\\ \ddot{\boldsymbol{x}}_2\\ \vdots\\ \ddot{\boldsymbol{x}}_{l-1}\\ \dot{\boldsymbol{\nu}}\end{bmatrix}. \tag{17}$$

Consequently, using (6) and (11) the ith level decoupled dynamic is realized as

$$\bar{\boldsymbol{\Lambda}}_i(\boldsymbol{q})\ddot{\tilde{\boldsymbol{x}}}_i + \bar{\boldsymbol{\mu}}_i(\boldsymbol{q},\dot{\boldsymbol{q}}) + \bar{\boldsymbol{p}}_i(\boldsymbol{q}) = \bar{\boldsymbol{f}}_{control,i} - \bar{\boldsymbol{J}}_i^{\#^T}(\boldsymbol{q})\boldsymbol{\tau}_{ext}, \tag{18}$$

where $\bar{\boldsymbol{\Lambda}}_i(\boldsymbol{q})$, $\bar{\boldsymbol{\mu}}_i(\boldsymbol{q})$ and $\bar{\boldsymbol{p}}_i(\boldsymbol{q})$ are computed by replacing $\boldsymbol{J}_i$ and $\boldsymbol{J}_i^{\#}$ with $\bar{\boldsymbol{J}}_i$ and $\bar{\boldsymbol{J}}_i^{\#}$ in (4) and (3), respectively. Moreover, $\boldsymbol{\tau} = \Sigma_{i=1}^{i=l}\bar{\boldsymbol{J}}_i^T(\boldsymbol{q})\bar{\boldsymbol{f}}_{control,i}$. It is noteworthy that for the force control task, $-\boldsymbol{f}_f$ which is the force

vector applied to the force control task space should be added to the right side of (18).

Thanks to the Jacobian definition in (6), $n_l = n - \sum_{i=1}^{l-1} n_i$, and l decoupled task space dynamics (similar to (18)) can be obtained which facilitate the control of several tasks, simultaneously. Moreover, the null space dynamics is in clear form and it is possible to handle the physical interactions besides accomplishing the tasks. In other words, a compliance behavior can be obtained during physical interaction in the null space. It is noteworthy that according to the comparison between different methods for defining orientation error reported in Caccavale, Natale, Siciliano, and Villani (1998), the unit quaternion formulation is employed for orientation tasks in the present work.

Denoting the command acceleration in the ith task space with $\ddot{\boldsymbol{x}}_{c,i}$ and in the null space by $\dot{\boldsymbol{\nu}}_c$, the control torques can be computed through

$$\begin{aligned}\boldsymbol{\tau} = &\sum_{i=1}^{l-1} \bar{\boldsymbol{J}}_i^T(\bar{\boldsymbol{\Lambda}}_i(\ddot{\boldsymbol{x}}_{c,i} - \dot{\bar{\boldsymbol{J}}}_i\dot{\boldsymbol{q}})) + \bar{\boldsymbol{J}}_l^T(\bar{\boldsymbol{\Lambda}}_l(\dot{\boldsymbol{\nu}}_c - \dot{\bar{\boldsymbol{J}}}_l\dot{\boldsymbol{q}}))\\ &+ \boldsymbol{J}_f^T\boldsymbol{f}_f + \boldsymbol{C}\dot{\boldsymbol{q}} + \boldsymbol{g}.\end{aligned} \tag{19}$$

Considering (11), (18) and (19), one can simplifies the task space closed-loop dynamics as

$$\bar{\boldsymbol{\Lambda}}_i[\ddot{\tilde{\boldsymbol{x}}} - \ddot{\boldsymbol{x}}_c + \bar{\boldsymbol{J}}_i\boldsymbol{M}^{-1}\boldsymbol{\tau}_{ext}] = \boldsymbol{0}, \tag{20}$$

which clearly shows the significant effect of the external physical interaction torque on the robot performance. The major issues in the following section are:

- Proposing controller–observer for accurate, efficient and safe force, position and orientation control along with compliance in the null space.
- Discussing the stability of the manipulator by employing new force, position and orientation control commands besides the method proposed in Sadeghian et al. (2013) for position control in any arbitrary task combination.

4. Controller design and stability

In this section, we propose a new controller–observer algorithm based on the *generalized momentum observer*. In our previous work (Sadeghian et al., 2014), the generalized momentum observer, originally proposed in De Luca and Mattone (2005), has been exploited effectively to control the interaction during task space control. In that work, we mainly considered the regulation of the task space position around a desired position. Here a novel method for controlling force and orientation tasks is proposed. Meanwhile, the stability analysis covers multiple force, orientation and position control or any combination of them besides compliance in the null space. The Jacobian definition in (6) and the analysis in the previous section enable us to achieve this goal, properly.

4.1. Controller design

By using the dynamics (1), n-dimensional residual vector $\boldsymbol{r}$ is defined as

$$\boldsymbol{r}(t) = \boldsymbol{K}_{obs}[\boldsymbol{p}(t) - \int_0^t (\boldsymbol{\tau} + \boldsymbol{C}^T\dot{\boldsymbol{q}} - \boldsymbol{g} - \boldsymbol{J}_f^T\boldsymbol{f}_f + \boldsymbol{r}(\sigma))d\sigma], \tag{21}$$

where $\boldsymbol{p}(t) = \boldsymbol{M}\dot{\boldsymbol{q}}$, $\boldsymbol{p}(0) = \boldsymbol{0}$, $\boldsymbol{r}(0) = \boldsymbol{0}$ and $\boldsymbol{K}_{obs} \in \mathbb{R}^{n\times n}$ is a positive definite matrix. It can be shown that the residual vector dynamics is

$$\dot{\boldsymbol{r}} = -\boldsymbol{K}_{obs}\boldsymbol{r} - \boldsymbol{K}_{obs}\boldsymbol{\tau}_{ext}. \tag{22}$$

Hence, by choosing proper gain $\boldsymbol{K}_{obs}$, the accidental physical interactions with the robot body can be estimated through (21). Note that the intentional interaction with the robot body for force control task ($\boldsymbol{f}_f$) is not included in the realized estimation.

Observing (20), it is obvious that any accidental contact with the robot body may produce deviation from the assigned task. Proper command acceleration can handle undesired motions and reduce the task errors. For accurate task execution, the command accelerations for force, position and orientation control are proposed as

$$\ddot{\boldsymbol{x}}_{cf} = \boldsymbol{K}_{f,p}\tilde{\boldsymbol{f}} + \boldsymbol{K}_{f,i}\int \tilde{\boldsymbol{f}}d\sigma - \boldsymbol{K}_{f,d}\dot{\tilde{\boldsymbol{x}}}_f - \bar{\boldsymbol{\Lambda}}_f^{-1}\bar{\boldsymbol{J}}_f^{\#T}\boldsymbol{r}, \tag{23}$$

$$\ddot{\boldsymbol{x}}_{cp} = -\boldsymbol{K}_{p,d}\dot{\tilde{\boldsymbol{x}}} + \boldsymbol{K}_{p,p}\tilde{\boldsymbol{x}} - \bar{\boldsymbol{\Lambda}}_p^{-1}\bar{\boldsymbol{J}}_p^{\#T}\boldsymbol{r}, \tag{24}$$

$$\ddot{\boldsymbol{x}}_{co} = -\boldsymbol{K}_{o,d}\bar{\boldsymbol{\omega}}_e + \boldsymbol{K}_{o,p}\boldsymbol{\varepsilon}_{de} - \bar{\boldsymbol{\Lambda}}_o^{-1}\bar{\boldsymbol{J}}_o^{\#T}\boldsymbol{r}. \tag{25}$$

Here, $\tilde{\boldsymbol{f}} = \boldsymbol{f}_d - \boldsymbol{f}_f$ is the force control error and $\dot{\tilde{\boldsymbol{x}}}_f$ is the velocity vector in the force control direction. $\boldsymbol{K}_{f,i} \in \mathbb{R}^{n_f\times n_f}$, $\boldsymbol{K}_{f,p} \in \mathbb{R}^{n_f\times n_f}$ and $\boldsymbol{K}_{f,d} \in \mathbb{R}^{n_f\times n_f}$ are positive definite gains in the force control space. For position control tasks, $\boldsymbol{x}$ is the task space variable and $\tilde{\boldsymbol{x}} = \boldsymbol{x}_d - \boldsymbol{x}$. In (25), $\bar{\boldsymbol{\omega}}_e$ and $\boldsymbol{\varepsilon}_{de}$ are the end effector angular velocity vector and the vector part of the quaternion parameters extracted from mutual rotation matrix $\boldsymbol{R}_d^e$ i. Moreover, $\boldsymbol{K}_{p,p} \in \mathbb{R}^{n_p\times n_p}$, $\boldsymbol{K}_{p,d} \in \mathbb{R}^{n_p\times n_p}$, $\boldsymbol{K}_{o,p} \in \mathbb{R}^{n_o\times n_o}$ and $\boldsymbol{K}_{o,d} \in \mathbb{R}^{n_o\times n_o}$ are positive definite matrices considered as position and orientation control gains and n_p and n_o are the corresponding task space dimensions.

Thanks to the robot redundancy, compliant behavior can be imposed in the null space of the major tasks with the null space command acceleration,

$$\dot{\boldsymbol{\nu}}_c = -\bar{\boldsymbol{\Lambda}}_l^{-1}((\bar{\boldsymbol{\mu}}_l + \boldsymbol{B}_l)\boldsymbol{\nu} - \boldsymbol{Z}_{l-1}\boldsymbol{K}_{l,p}\tilde{\boldsymbol{q}}), \tag{26}$$

where $\tilde{\boldsymbol{q}} = \boldsymbol{q}_d - \boldsymbol{q}$, and $\boldsymbol{q}_d \in \mathbb{R}^{n\times 1}$ as a desired joint space configuration and $\boldsymbol{B}_l \in \mathbb{R}^{n_l\times n_l}$ is a positive definite matrix. These command accelerations are further used in (19) to construct manipulator control torque.

Proposition 1. *Assume that the external torque ($\boldsymbol{\tau}_{ext}$) is constant (or slowly time varying). The control command (19) besides the command accelerations (23)–(26) and the residual vector (21) guarantee that the task space and torque estimation errors go to zero asymptotically. Moreover, a desired compliant behavior is imposed in the null space of the tasks.*

4.2. Stability analysis

In this section, the stability analysis of the proposed controller–observer is performed. First, some preliminary theorems and lemmas are given. Afterward, in Section 4.2.2 the above proposition is clarified and proved. Independent main tasks are considered in the stability. Task dependency are discussed separately at the end of the subsection.

4.2.1. Preliminary theorems

Theorem 2 (*Iggidr, Kalitine, & Outbib, 1996*)**.** *Consider the system $\dot{\boldsymbol{z}} = h(\boldsymbol{z})$ with $\boldsymbol{z} = 0$ as equilibrium point. If a function $V(\boldsymbol{z}) \in C^1(\Omega, \mathbb{R})$ on the neighborhood Ω of the origin exists such that,*

- *$V(\boldsymbol{z}) \geq 0$ for all $\boldsymbol{z} \in \Omega$ and $V(0) = 0$;*
- *$\dot{V}(\boldsymbol{z}) \leq 0$ for all $\boldsymbol{z} \in \Omega$;*
- *The system is asymptotically stable in the largest positively invariant set $\mathcal{L}$ contained in $\{\boldsymbol{z} \in \Omega | \dot{V}(\boldsymbol{z}) = 0\}$;*

the origin is then asymptotically stable.

Lemma 3 (*Khalil & Grizzle, 1996*)**.** *Consider the dynamical system $\dot{\boldsymbol{z}} = f(\boldsymbol{z}, t) + d(\boldsymbol{z}, t)$ where $f(\boldsymbol{z}, t)$ is the nominal system and $d(\boldsymbol{z}, t)$ is the perturbation term. Let $\boldsymbol{z} = 0$ be an exponentially stable equilibrium point for the nominal system ($\dot{\boldsymbol{z}} = f(\boldsymbol{z}, t)$) and $V(\boldsymbol{z}, t)$ be a Lyapunov function for the nominal system such that*

$$C_1\|\boldsymbol{z}\|^2 \leq V(\boldsymbol{z}, t) \leq C_2\|\boldsymbol{z}\|^2, \tag{27}$$

$$\frac{\partial V}{\partial t} + \frac{\partial V}{\partial \boldsymbol{z}}f(\boldsymbol{z}) \leq -C_3\|\boldsymbol{z}\|^2, \tag{28}$$

$$\|\frac{\partial V}{\partial \boldsymbol{z}}\| \leq C_4\|\boldsymbol{z}\|, \tag{29}$$

and the perturbation term $d(z,t)$ satisfies

$$\|d(z,t)\| \leq \gamma\|z\|. \tag{30}$$

Considering,

$$\begin{aligned}\dot{V}(z) &= \frac{\partial V}{\partial t} + \frac{\partial V}{\partial z} f(z) + \frac{\partial V}{\partial z} d(z,t) \\ &\leq -C_3\|z\|^2 + \frac{\partial V}{\partial z}\|d(z,t)\| \\ &\leq -C_3\|z\|^2 + C_4\gamma\|z\|^2 \\ &\leq -(C_3 - \gamma C_4)\|z\|^2,\end{aligned} \tag{31}$$

the system is exponentially stable if γ is small enough to satisfy the bound

$$\gamma \leq \frac{C_3}{C_4}. \tag{32}$$

4.2.2. Stability proof

The stability proof is based on *Conditional Stability Theorem* (Theorem 2). Without loss of generality, let's consider the force control as the first priority task and position control and orientation control as the second and third priority tasks, respectively. The remaining degrees of freedom is also assumed to be exploited in the null space by (26).

Proof of Proposition 1. By replacing (23)–(19) in the robot dynamics (18), the closed loop dynamics for the main tasks as well as the null space dynamics are obtained as,

$$-\ddot{\tilde{\boldsymbol{x}}}_f - \boldsymbol{K}_{f,d}\dot{\tilde{\boldsymbol{x}}}_f + \boldsymbol{K}_{f,p}\tilde{\boldsymbol{f}} + \boldsymbol{K}_{f,i}\int_0^t \tilde{\boldsymbol{f}}\,d\sigma = \bar{\boldsymbol{\Lambda}}_f^{-1}\bar{\boldsymbol{J}}_f^{\#T}\tilde{\boldsymbol{r}}, \tag{33}$$

$$-\ddot{\tilde{\boldsymbol{x}}} - \boldsymbol{K}_{p,d}\dot{\tilde{\boldsymbol{x}}} + \boldsymbol{K}_{p,p}\tilde{\boldsymbol{x}} = \bar{\boldsymbol{\Lambda}}_p^{-1}\bar{\boldsymbol{J}}_p^{\#T}\tilde{\boldsymbol{r}}, \tag{34}$$

$$-\dot{\tilde{\boldsymbol{\omega}}}_e - \boldsymbol{K}_{o,d}\tilde{\boldsymbol{\omega}}_e + \boldsymbol{K}_{o,p}\boldsymbol{\varepsilon}_{de} = \bar{\boldsymbol{\Lambda}}_o^{-1}\bar{\boldsymbol{J}}_o^{\#T}\tilde{\boldsymbol{r}}, \tag{35}$$

$$-\bar{\boldsymbol{\Lambda}}_l\dot{\boldsymbol{\nu}} - (\bar{\boldsymbol{\mu}}_l + \bar{\boldsymbol{B}}_l)\boldsymbol{\nu} + \boldsymbol{Z}_{l-1}\boldsymbol{K}_{l,p}\tilde{\boldsymbol{q}} = \boldsymbol{Z}_{l-1}\boldsymbol{\tau}_{ext}. \tag{36}$$

Additionally, considering the estimation error as $\tilde{\boldsymbol{r}} = \boldsymbol{r} + \boldsymbol{\tau}_{ext}$, (22) can be rewritten as,

$$\dot{\tilde{\boldsymbol{r}}} + \boldsymbol{K}_{obs}\tilde{\boldsymbol{r}} = \dot{\boldsymbol{\tau}}_{ext}. \tag{37}$$

Consequently, the closed loop dynamics of the system is constructed by (9), (33)–(37) as well as the propagation dynamics, Siciliano, Sciavicco, and Villani (2010)

$$\dot{\eta}_{de} = -\frac{1}{2}\boldsymbol{\varepsilon}_{de}^{eT}\tilde{\boldsymbol{\omega}}_{de}^{e}, \tag{38}$$

$$\dot{\boldsymbol{\varepsilon}}_{de}^{e} = \frac{1}{2}E(\eta_{de}, \boldsymbol{\varepsilon}_{de}^{eT})\tilde{\boldsymbol{\omega}}_{de}^{e}, \tag{39}$$

where $\boldsymbol{\varepsilon}_{de} = \boldsymbol{R}_e\boldsymbol{\varepsilon}_{de}^{e}$, and $\tilde{\boldsymbol{\omega}}_{de}^{e} = \boldsymbol{\omega}_d^e - \bar{\boldsymbol{\omega}}_e^e$, considering the desired angular velocity $\boldsymbol{\omega}_d^e$ to be zero. According to the assigned priorities for the stability proof and the definition given in (7), $\bar{\boldsymbol{J}}_f = \bar{\boldsymbol{J}}_1$, $\bar{\boldsymbol{J}}_p = \bar{\boldsymbol{J}}_2$ and $\bar{\boldsymbol{J}}_o = \bar{\boldsymbol{J}}_3$.

The environment stiffness ($\boldsymbol{K}_{env}$) and damping ($\boldsymbol{C}_{env}$) are assumed to be unknown positive quantities. Thus, the applied force on the environment and the desired force are given as follows,

$$\boldsymbol{f}_f = \boldsymbol{K}_{env}(\boldsymbol{x}_f - \boldsymbol{x}_{initial}) + \boldsymbol{C}_{env}\dot{\boldsymbol{x}}_f, \tag{40}$$

$$\boldsymbol{f}_d = \boldsymbol{K}_{env}(\boldsymbol{x}_d - \boldsymbol{x}_{initial}). \tag{41}$$

It should be noted that the desired position $\boldsymbol{x}_d$ is unknown. However, for each desired force it has a specific value. One can replace $\tilde{\boldsymbol{f}}$ in (33) with $\boldsymbol{K}_{env}\tilde{\boldsymbol{x}}_f - \boldsymbol{C}_{env}\dot{\boldsymbol{x}}_f$, where $\tilde{\boldsymbol{x}}_f = \boldsymbol{x}_d - \boldsymbol{x}_f$. Since, for independent tasks $\bar{\boldsymbol{x}}_i = \boldsymbol{x}_i$, $\boldsymbol{x}_f$ can be replaced with $\bar{\boldsymbol{x}}_f$ in $\tilde{\boldsymbol{x}}_f$ as well as $\boldsymbol{x}$ with $\bar{\boldsymbol{x}}$ in $\tilde{\boldsymbol{x}}$.

The state space vector of the closed loop system is $\boldsymbol{z} = (\dot{\tilde{\boldsymbol{x}}}, \tilde{\boldsymbol{x}}, \dot{\tilde{\boldsymbol{x}}}_f, \tilde{\boldsymbol{x}}_f, \int_0^t \tilde{\boldsymbol{x}}_f\,d\sigma, \bar{\boldsymbol{\omega}}_e, \boldsymbol{\varepsilon}_{de}, \eta_{de}, \boldsymbol{\nu}, \tilde{\boldsymbol{q}})$. At the first step, the stability of the force task in addition to the observer estimation error dynamics are investigated. Eqs. (33) and (37) can be considered as perturbed linear system,

$$\dot{\boldsymbol{z}} = \boldsymbol{A}\boldsymbol{z} + d(z,t), \tag{42}$$

when the external force is assumed to be constant (or slowly time varying). One should consider that this assumption is held during force control since f_f is independent from $\boldsymbol{\tau}_{ext}$ (see (1), (3), (21)). In (42), the perturbation term for nonsingular manipulator configuration is bounded as

$$\|\bar{\boldsymbol{\Lambda}}_f^{-1}\bar{\boldsymbol{J}}_f^{\#T}\tilde{\boldsymbol{r}}\| \leq \gamma\|z\|. \tag{43}$$

Therefore, $d(z,t)$ in (42) satisfies (30). By properly choosing the control gains in (23), a negative definite matrix $\boldsymbol{A}$ can be obtained in (30). Hence, the quadratic function

$$V_1(z) = \frac{1}{2}[(\int_0^t \tilde{\boldsymbol{x}}_f\,d\sigma)^T\ \tilde{\boldsymbol{x}}_f^T\ \dot{\tilde{\boldsymbol{x}}}_f^T\ \tilde{\boldsymbol{r}}^T]\boldsymbol{P}\begin{bmatrix}\int_0^t \tilde{\boldsymbol{x}}_f\,d\sigma \\ \tilde{\boldsymbol{x}}_f \\ \dot{\tilde{\boldsymbol{x}}}_f \\ \tilde{\boldsymbol{r}}\end{bmatrix}, \tag{44}$$

is exploited in this step where $\boldsymbol{P}$ is a positive definite matrix that fulfills $\boldsymbol{P}\boldsymbol{A} + \boldsymbol{A}^T\boldsymbol{P} = -\boldsymbol{I}$ (Khalil & Grizzle, 1996). The time derivative of (44) along the solutions of (33) and (37) yields

$$\begin{aligned}\dot{V}_1(z) &= \frac{\partial V}{\partial z} f(z) + \frac{\partial V}{\partial z} g(t,z) \\ &= -\dot{\tilde{\boldsymbol{x}}}_f^T\dot{\tilde{\boldsymbol{x}}}_f - \tilde{\boldsymbol{x}}_f^T\tilde{\boldsymbol{x}}_f - (\int_0^t \tilde{\boldsymbol{x}}_f\,d\sigma)^T(\int_0^t \tilde{\boldsymbol{x}}_f\,d\sigma) - \tilde{\boldsymbol{r}}^T\tilde{\boldsymbol{r}} \\ &\quad - \bar{\boldsymbol{\Lambda}}_f^{-1}\bar{\boldsymbol{J}}_f^{\#T}\boldsymbol{\mathcal{H}}(\int_0^t \tilde{\boldsymbol{x}}_f\,d\sigma, \dot{\tilde{\boldsymbol{x}}}_f, \tilde{\boldsymbol{x}}_f).\end{aligned} \tag{45}$$

where the second line in (45) shows exponential stability of the nominal system and the third line is related to the perturbation term. Since the nominal system in (42) is exponentially stable and (43) holds, by observing Lemma 3 we realize that (44) and (45) fulfills the first two conditions of Theorem 2. For the last condition, asymptotic stability of the system conditionally to set $\Sigma_1 = \{\boldsymbol{z}|\dot{V}_1(\boldsymbol{z}) = 0\} = \{\dot{\tilde{\boldsymbol{x}}}, \tilde{\boldsymbol{x}}, \bar{\boldsymbol{\omega}}_e, \boldsymbol{\varepsilon}_{de}, \boldsymbol{\eta}_{de}, \tilde{\boldsymbol{q}}, \boldsymbol{\nu}, \dot{\tilde{\boldsymbol{x}}}_f = \boldsymbol{0}, \tilde{\boldsymbol{x}}_f = \boldsymbol{0}, \int_0^t \tilde{\boldsymbol{x}}_f\,d\sigma = \boldsymbol{0}, \tilde{\boldsymbol{r}} = \boldsymbol{0}\}$ must be shown (see Fig. 3). By selecting proper gain matrices in (24) and employing *Lyapunov* equation similar to the previous step, one can realize the function

$$\begin{aligned}V_2(z) =& \frac{1}{2}\tilde{\boldsymbol{x}}^T(\boldsymbol{K}_{p,d}\boldsymbol{K}_{p,p}{}^{-1} + \boldsymbol{K}_{p,d}{}^{-1}\boldsymbol{K}_{p,p} + \boldsymbol{K}_{p,d}{}^{-1})\tilde{\boldsymbol{x}} \\ &+ \frac{1}{2}\dot{\tilde{\boldsymbol{x}}}^T(\boldsymbol{I} + \boldsymbol{K}_{p,p}{}^{-1})\boldsymbol{K}_{p,d}^{-1}\dot{\tilde{\boldsymbol{x}}} + \dot{\tilde{\boldsymbol{x}}}^T\boldsymbol{K}_{p,p}{}^{-1}\tilde{\boldsymbol{x}},\end{aligned} \tag{46}$$

which is positive semi-definite within Σ_1. The time derivative of (46) using (34) is simplified as

$$\dot{V}_2(z) = -\dot{\tilde{\boldsymbol{x}}}^T\dot{\tilde{\boldsymbol{x}}} - \tilde{\boldsymbol{x}}^T\tilde{\boldsymbol{x}}. \tag{47}$$

Since (47) is negative semi-definite, to show the asymptotic stability of this subset (Σ_1) using Theorem 2, we should investigate the asymptotic stability in the subset $\Sigma_2 = \{(\dot{\tilde{\boldsymbol{x}}}, \tilde{\boldsymbol{x}}, \bar{\boldsymbol{\omega}}_e, \boldsymbol{\varepsilon}_{de}, \boldsymbol{\eta}_{de}, \tilde{\boldsymbol{q}}, \boldsymbol{\nu}, \dot{\tilde{\boldsymbol{x}}}_f = \boldsymbol{0}, \tilde{\boldsymbol{x}}_f = \boldsymbol{0}, \int_0^t \tilde{\boldsymbol{x}}_f\,d\sigma = \boldsymbol{0}, \tilde{\boldsymbol{r}} = \boldsymbol{0})|\dot{V}_2(\boldsymbol{z}) = 0\}$. Exploiting *Lyapunov* function candidate,

$$V_3(z) = \boldsymbol{K}_{o,p}((\eta_{de} - 1)^2 + \boldsymbol{\varepsilon}_{de}^T\boldsymbol{\varepsilon}_{de}) + \frac{1}{2}\bar{\boldsymbol{\omega}}_e^T\bar{\boldsymbol{\omega}}_e, \tag{48}$$

and by (38)–(39) we realize,

$$\begin{aligned}\dot{V}_3(z) &= 2\boldsymbol{K}_{o,p}((\eta_{de} - 1)\dot{\eta}_{de} + \boldsymbol{\varepsilon}_{de}^T\dot{\boldsymbol{\varepsilon}}_{de}) + \dot{\bar{\boldsymbol{\omega}}}_e^T\bar{\boldsymbol{\omega}}_e \\ &= -\boldsymbol{K}_{o,d}\bar{\boldsymbol{\omega}}_e^T\bar{\boldsymbol{\omega}}_e.\end{aligned} \tag{49}$$

Obviously, $V_3(z)$ and $\dot{V}_3(z)$ satisfy conditional stability prerequisites along the system trajectories. As a result, the last subset is realized as $\Sigma_{l-1} = \Sigma_3 = \{\tilde{\boldsymbol{q}}, \boldsymbol{\nu}, \boldsymbol{\varepsilon}_{de}, \eta_{de}, \dot{\tilde{\boldsymbol{x}}} = \boldsymbol{0}, \tilde{\boldsymbol{x}} = \boldsymbol{0}, \dot{\tilde{\boldsymbol{x}}}_f = \boldsymbol{0}, \tilde{\boldsymbol{x}}_f = \boldsymbol{0}, \int_0^t \tilde{\boldsymbol{x}}_f\,d\sigma = \boldsymbol{0}, \tilde{\boldsymbol{r}} = \boldsymbol{0}, \bar{\boldsymbol{\omega}}_e = \boldsymbol{0}\}$. In this set, for the case of non zero accidental external torque ($\boldsymbol{\tau}_{ext}$) and $\boldsymbol{x}(\boldsymbol{q}_d) \neq \boldsymbol{x}_d$, the asymptotic stability can be proven as follows. The equilibrium point for the system in this case is $\{\boldsymbol{q} = \boldsymbol{q}^*, \boldsymbol{\nu} = \boldsymbol{0}, \dot{\tilde{\boldsymbol{x}}} = \boldsymbol{0}, \tilde{\boldsymbol{x}} = \boldsymbol{0}, \dot{\tilde{\boldsymbol{x}}}_f = \boldsymbol{0}, \tilde{\boldsymbol{x}}_f = \boldsymbol{0}, \int_0^t \tilde{\boldsymbol{x}}_f\,d\sigma = \boldsymbol{0}, \tilde{\boldsymbol{r}} = \boldsymbol{0}, \bar{\boldsymbol{\omega}} = \boldsymbol{0}, \boldsymbol{\varepsilon}_{de} = \boldsymbol{0}, \eta_{de} = 1\}$ where $\boldsymbol{q}^*$ is a solution of

$$\boldsymbol{Z}_{l-1}(\boldsymbol{K}_{l,p}\tilde{\boldsymbol{q}} - \boldsymbol{\tau}_{ext}) = \boldsymbol{0}, \tag{50}$$

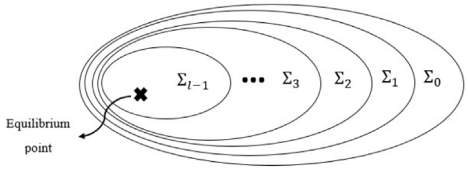

Fig. 3. Nested sets used for stability proof in the state space. Σ_0 is the complete and unrestricted state space z. By employing the conditional stability theorem for the ith step, a new subset Σ_i is created where the stability of the next step is studied inside this subset.

and is compatible with the previous tasks. The result locally minimizes the function $\|\boldsymbol{K}_{l,p}\tilde{\boldsymbol{q}} - \boldsymbol{\tau}_{ext}\|^2$ w.r.t $\boldsymbol{x}_i(\boldsymbol{q}) = \boldsymbol{x}_{i,d}$. More details about computing $\boldsymbol{q}^*$ can be found in Chang (1987) and Sadeghian et al. (2014). The proof of asymptotic stability of the equilibrium point of the system is based on the function

$$V_l = \boldsymbol{K}_{o,p}((\eta_{de}-1)^2 + \boldsymbol{\epsilon}_{de}^T\boldsymbol{\epsilon}_{de}) + \frac{1}{2}\boldsymbol{\nu}^T\bar{\boldsymbol{\Lambda}}_l\boldsymbol{\nu} + \frac{1}{2}\tilde{\boldsymbol{q}}^{*T}\boldsymbol{K}_{l,p}\tilde{\boldsymbol{q}}^*, \tag{51}$$

where $\tilde{\boldsymbol{q}}^* = \boldsymbol{q}^* - \boldsymbol{q}$. Within the set $\boldsymbol{\Sigma}_{l-1}$, the joint space velocity is $\dot{\boldsymbol{q}} = \bar{\boldsymbol{J}}_l\boldsymbol{\nu}$ and the time derivative of V_l can be computed as,

$$\begin{aligned}\dot{V}_l =& -\boldsymbol{\nu}^T(\bar{\boldsymbol{\mu}}_l + \boldsymbol{B}_l)\boldsymbol{\nu} + \boldsymbol{\nu}^T\boldsymbol{Z}_{l-1}\boldsymbol{K}_{l,p}\tilde{\boldsymbol{q}} - \boldsymbol{\nu}^T\boldsymbol{Z}_{l-1}\boldsymbol{\tau}_{ext}\\ &- \boldsymbol{\nu}^T\boldsymbol{Z}_{l-1}\boldsymbol{K}_{l,p}\tilde{\boldsymbol{q}}^* + 2\boldsymbol{K}_{o,p}((\eta_{de}-1)\dot{\eta}_{de} + \boldsymbol{\epsilon}_{de}^T\dot{\boldsymbol{\epsilon}}_{de})\\ =& -\boldsymbol{\nu}^T(\bar{\boldsymbol{\mu}}_l + \boldsymbol{B}_l)\boldsymbol{\nu}.\end{aligned} \tag{52}$$

Note that in the current set $\bar{\boldsymbol{\omega}}_e$ is zero, implying that $\dot{\eta}$ and $\dot{\boldsymbol{\epsilon}}_{de}$ are null. Considering La Salle's invariance principal, the state of the system converges to the largest invariant set with $\boldsymbol{\nu} = \boldsymbol{0}$ in Σ_{l-1}. By observing the system closed loop equations beside (50), the invariant set is realized as $\{\boldsymbol{q} = \boldsymbol{q}^*, \boldsymbol{\nu} = \boldsymbol{0}, \dot{\tilde{\boldsymbol{x}}} = \boldsymbol{0}, \tilde{\boldsymbol{x}} = \boldsymbol{0}, \dot{\tilde{\boldsymbol{x}}}_f = \boldsymbol{0}, \tilde{\boldsymbol{x}}_f = \boldsymbol{0}, \int_0^t \tilde{\boldsymbol{x}}_f d\sigma = \boldsymbol{0}, \tilde{\boldsymbol{r}} = \boldsymbol{0}, \bar{\boldsymbol{\omega}} = \boldsymbol{0}, \boldsymbol{\epsilon}_{de} = \boldsymbol{0}, \eta_{de} = 1\}$. It is noteworthy that there is another equilibrium point for the system as $\{\boldsymbol{q} = \boldsymbol{q}^*, \boldsymbol{\nu} = \boldsymbol{0}, \dot{\tilde{\boldsymbol{x}}} = \boldsymbol{0}, \tilde{\boldsymbol{x}} = \boldsymbol{0}, \dot{\tilde{\boldsymbol{x}}}_f = \boldsymbol{0}, \tilde{\boldsymbol{x}}_f = \boldsymbol{0}, \int_0^t \tilde{\boldsymbol{x}}_f d\sigma = \boldsymbol{0}, \tilde{\boldsymbol{r}} = \boldsymbol{0}, \boldsymbol{\omega}_e = \boldsymbol{0}, \boldsymbol{\epsilon}_{de} = \boldsymbol{0}, \eta_{de} = -1\}$ which is unstable. This can be shown by taking a small perturbation around this equilibrium point. Let $\eta_{de} = -1 + \sigma$ and $\sigma > 0$ and consider that unit quaternion parameters are constrained as

$$\eta^2 + \boldsymbol{\epsilon}^T\boldsymbol{\epsilon} = 1. \tag{53}$$

Perturbed V_l simplifies to $V_{l_\sigma} = 4\boldsymbol{K}_{o,p} - 2\sigma\boldsymbol{K}_{o,p}$ while V_l for the equilibrium point is $V_{l,eq} = 4\boldsymbol{K}_{o,p}$. By (52), V_l is decreasing and will never return to $V_{l,eq}$ from $V_{l,\sigma}$. Thus, we can infer that this equilibrium point is unstable (similar analysis can be found in Caccavale et al. (1998)).

When $\boldsymbol{\tau}_{ext} = \boldsymbol{0}$, the asymptotic stability is preserved while the system converges to new equilibrium point for $\boldsymbol{q}$ and the equilibrium set is $\{\boldsymbol{q} = \boldsymbol{q}_d, \boldsymbol{\nu} = \boldsymbol{0}, \dot{\tilde{\boldsymbol{x}}} = \boldsymbol{0}, \tilde{\boldsymbol{x}} = \boldsymbol{0}, \dot{\tilde{\boldsymbol{x}}}_f = \boldsymbol{0}, \tilde{\boldsymbol{x}}_f = \boldsymbol{0}, \int_0^t \tilde{\boldsymbol{x}}_f d\sigma = \boldsymbol{0}, \tilde{\boldsymbol{r}} = \boldsymbol{0}, \boldsymbol{\omega}_e = \boldsymbol{0}, \boldsymbol{\epsilon}_{de} = \boldsymbol{0}, \eta_{de} = 1\}$. Therefore, by virtue of Theorem 2, Σ_3 is asymptotically stable. Subsequently, the third condition of this theorem in the subsets Σ_2 and Σ_1 is satisfied and thus the asymptotic convergence to the equilibrium point of the system is achieved.

Remark 1. An alternative scheme to show the system stability is to replace V_1 with two positive semi-definite functions V_{obs} and V_f. Consider that,

$$V_{obs} = \frac{1}{2}\tilde{\boldsymbol{r}}^T\tilde{\boldsymbol{r}}, \tag{54}$$

and its time derivative along the system trajectory as

$$\dot{V}_{obs} = -\dot{\tilde{\boldsymbol{r}}}^T\boldsymbol{K}_{obs}\dot{\tilde{\boldsymbol{r}}}, \tag{55}$$

at the first step. Hence, the stability analysis of the system should be discussed in the subset $\Sigma_{obs} = \{\boldsymbol{z}|\dot{V}_{obs}(\boldsymbol{z}) = 0\} = \{\dot{\tilde{\boldsymbol{x}}}, \tilde{\boldsymbol{x}}, \bar{\boldsymbol{\omega}}_e, \boldsymbol{\epsilon}_{de}, \boldsymbol{\eta}_{de}, \tilde{\boldsymbol{q}}, \boldsymbol{\nu}, \dot{\tilde{\boldsymbol{x}}}_f, \tilde{\boldsymbol{x}}_f, \int_0^t \tilde{\boldsymbol{x}}_f d\sigma, \tilde{\boldsymbol{r}} = \boldsymbol{0}\}$. One can propose proper V_f to show the stability of the force control task by using Lyapunov equation. To this end, matrix $\boldsymbol{P}$ in $\boldsymbol{P}\boldsymbol{A} + \boldsymbol{A}^T\boldsymbol{P} = -\boldsymbol{I}$ should be computed according to $\boldsymbol{A}$ which is realized from (33) in the subset Σ_{obs}. This way, the Lemma 3 is not employed anymore. The rest of the stability analysis is the same as before.

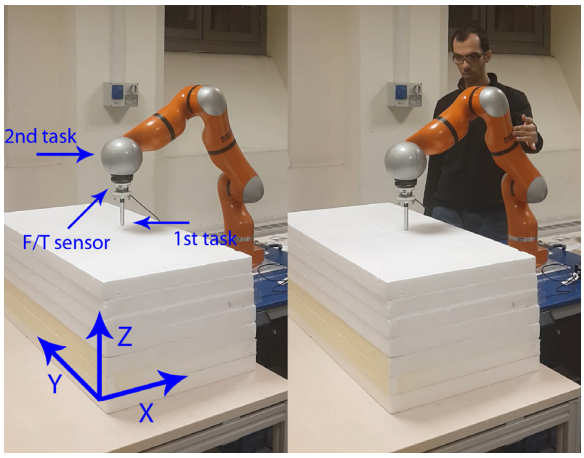

Fig. 4. Case I: The experimental setup during manipulation.

Remark 2. If multiple similar tasks are considered for manipulation, similar structure of V_2, V_3 and V_f can be employed for the tasks in the realized subsets. On the other hand, the stability analysis of the hybrid tasks is possible through the summation of the corresponding Lyapunov functions.

Remark 3. According to (20), if the considered tasks are dependent, the lower priority task is realized as much as possible in the sense of least-squares. In other words, the norm of $\|\ddot{\tilde{\boldsymbol{x}}} - \ddot{\boldsymbol{x}}_c + \bar{\boldsymbol{J}}_i M^{-1}\boldsymbol{\tau}_{ext}\|$ is minimized subject to the higher priority tasks. Since the observer performance is independent of the allocated priorities, the effect of $\boldsymbol{\tau}_{ext}$ is certainly compensated.

Remark 4. Because of using pseudoinverse in the solution, singularity may arise when the manipulator moves from a nonsingular configuration to a singular configuration. Damped Least-Squares (DLS) method is usually employed to treat this condition. Using DLS for the second-order kinematic control is discussed in Caccavale, Chiaverini, and Siciliano (1997). However, occurring this case is not common in the regulation tasks which are considered here.

5. Experimental evaluation

The proposed approach is verified experimentally on a 7DOF KUKA LWR robot arm. Various robot control approaches are investigated through this manipulator (Ajoudani, Tsagarakis, & Bicchi, 2011; Jin & Li, 2018; Mashayekhi, Behbahani, Ficuciello, & Siciliano, 2018). Moreover, a six axis Force/Torque sensor (ATI Mini-45) is mounted at the end-effector of the robot to measure the forces applied on the tip (Fig. 4).

Each scenario comprises two prioritized tasks in addition to the compliance behavior at the third level. Control algorithms are executed through fast research interface library (FRI) on a remote PC. Three experimental scenarios are devised. Corresponding command accelerations are used in (19) to obtain the desired behavior for the tasks along with the null space compliance. Some implementation details and exploited numerical methods are discussed in Appendix A.The videos related to the experiments reported in this section can be found as supplementary materials in online resource (Appendix B).

5.1. Case I

In this case, hybrid force–position control is considered as the first priority task and the position control is set as the second priority task. This combination of the tasks is useful for both humanoid robots and manipulators during complex manipulations. Humanoids can preserve their

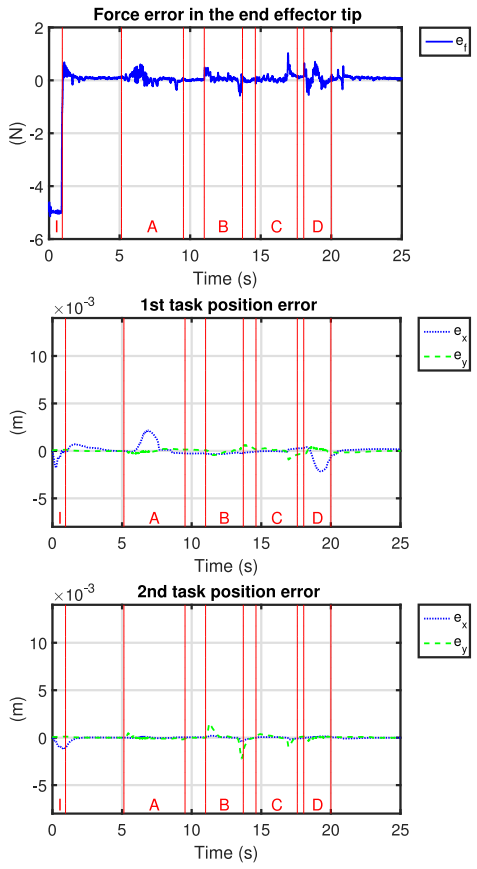

Fig. 5. Case I: First task force error (Top) and position error (Middle). Second task position error (Bottom). "I" corresponds to the initial interval where robot moves toward the platform. "A", "B", "C" and "D" show the intervals where human applies external interaction on the robot body.

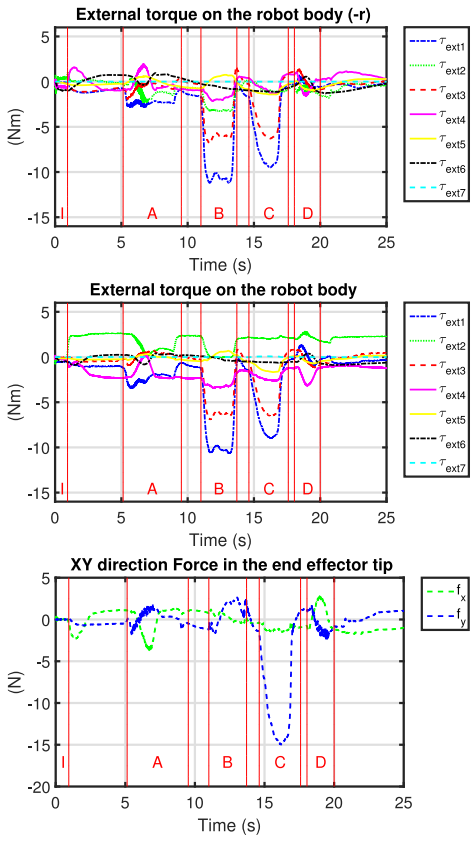

Fig. 6. Case I: External torques applied to the robot body computed by (21) (Top) and by internal torque sensors (Middle). The force magnitude at the end effector in X and Y directions (f_x and f_y) evaluated by the force sensor (Bottom).

stability by proper force control on their foots (and even another point of contacts) while executing other tasks using their redundancy (examples can be found in Khatib and Chung (2014) and Sentis et al. (2010)). Minimally Invasive Robotic Surgery (MIRS) (Sadeghian, Zokaei, & Jazi, 2018) is another example where the robot needs to apply accurate force by the end point of surgical tools while passing through a small incision.

In the current experiment, the initial robot configuration is $\boldsymbol{q}_d = \{0, \pi/6, 0, -\pi/2, 0, \pi/3, 0\}$ and the desired task is to apply $f_z = -5\ N$ force with the end effector tip to a specific point of platform located at $\boldsymbol{x}_{d_1} = [-0.5378\ 0]$. The second task is to preserve the end of the 5th arm initial position in the XY plane during manipulation. Eqs. (23), (24) and (26) are used to obtain the desired behavior while external forces are applied to the robot body by a human. In order to protect the robot and force sensor from unexpected happenings, soft panels are used as the environment (Fig. 4).

The performance of the controller is illustrated in Fig. 5. Five intervals are shown in the figures related to this case (Figs. 5 and 6). "I" is the interval which robot moves toward the platform for applying force. During intervals "A", "B", "C" and "D", external forces are applied to the various points of the robot body by a human (see Fig. 4). However, during applying force by the tip of the end effector, undesired external forces exist in X and Y directions too (see Fig. 6). The magnitude of the external interaction estimated by both the robot internal torque sensor and by using (21) are shown in Fig. 6. The difference between these two vectors is related to the Z direction force at the tip of the end-effector. Note that in (21), the intentional torques are omitted from the residual vector.

Fig. 5 shows that the force magnitude converges to the desired value rapidly when it reaches the platform. Considering the interaction intervals shown in Fig. 5, it can be seen that the force and position errors are negligible during the external interaction.

For the sake of studying the effect of using the observer in our control scheme, this scenario is repeated with the same gains for the task space and null space acceleration command while the external torque compensation is omitted in (23) and (24). The results are shown in Figs. 7 and 8. Without using the observer, the force convergence rate decreases significantly when the end effector interacts with the platform (Fig. 7). We tried to apply external forces almost to the same points of the robot in both cases. As it can be seen from Figs. 7 and 6, the maximum amount of the external torques are almost the same.

Without using the observer, the force magnitude variations in the interaction intervals ("A", "B" and "C" in Fig. 7) are significantly higher than the case with controller–observer (Fig. 5). Furthermore, convergence rate to the desired value is too slow in comparison with the proposed approach. Position control errors in both first and second priority tasks increase by omitting the observer and it is non-null not only during the interaction phase but also after that (Fig. 6). It is noteworthy that the error increases much more for the second priority task in comparison to the first priority task.

5.2. Case II

Preserving the desired orientation is a critical issue, especially in robotic surgery and visual servoing. Consider the case where a surgery tool mounted at the end-effector passes through an incision point in an MIRS scenario. Meanwhile, it should preserve specified orientation for example to ensure the safety of neighbor organs, apply force in the

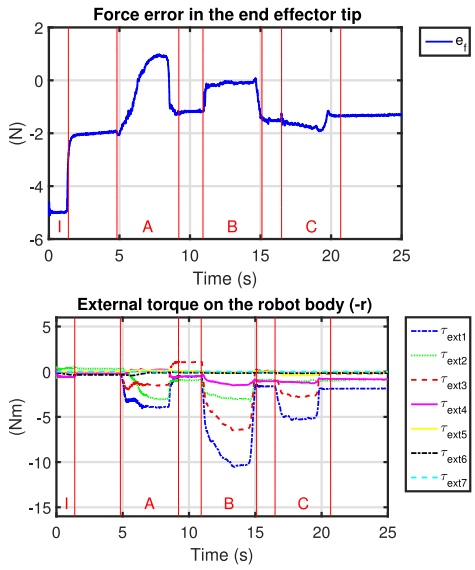

Fig. 7. Case I: Experimental results without using observer: First task force error (Top), External torque applied to the robot body (Bottom).

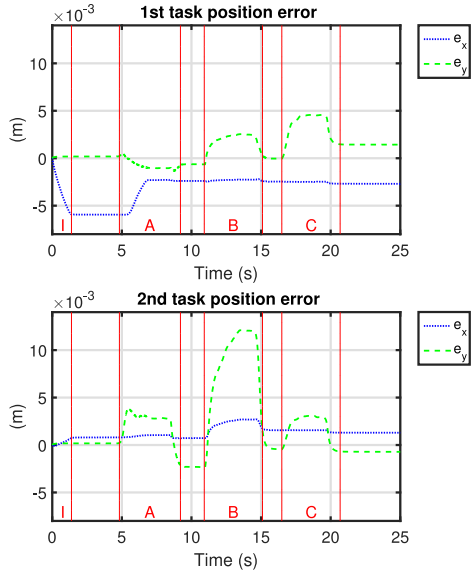

Fig. 8. Case I: Experimental results without using observer: First task position error (Top), Second task position error (Bottom).

specific direction or provide a special view in the endoscopic camera which is mounted at the robot end effector (Fig. 9). The current case studies the approach functionality in such scenarios.

In this set of experiments, the performance of the schemes for orientation control is studied by considering the end-effector orientation and the end of the 5th arm XY position as the first task (Fig. 10). The second task is the end effector position in Z direction. Robot initial configuration is $\boldsymbol{q}_i = \{0, \pi/6, 0, -\pi/2, \pi/6, -\pi/3, 0\}$ and it is commanded to show an impedance behavior when any external forces are applied to its body. The control command is computed by substituting (24)–(26) in (19).

The results are shown in Figs. 11 and 12. According to Section 4.2.2, η_{de} and ϵ_{de} should converge to 1 and $\mathbf{0}$, respectively. As it can be seen in Fig. 11, the deviation of the orientation parameters from the desired values is negligible during the interaction phases ("A", "B", "C" and "D"). Position tasks errors are significantly small and converge to zero when the external interaction is constant (see Fig. 12).

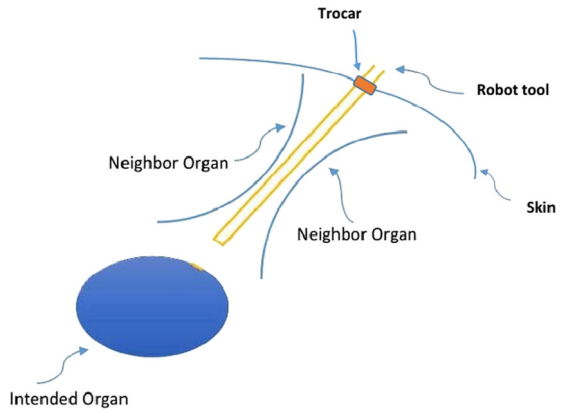

Fig. 9. Sample scenario for orientation control; a surgery tool mounted at the end-effector passes through an incision point in a MIRS scenario.

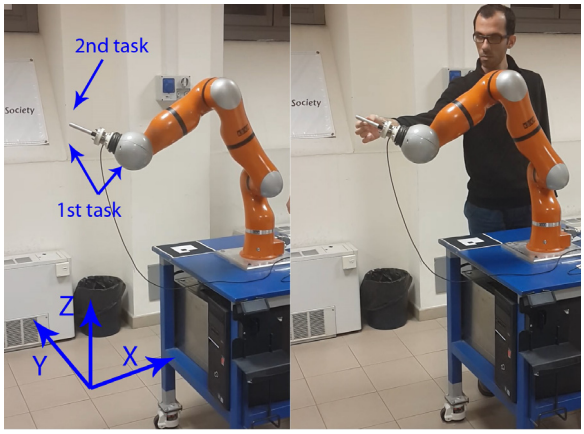

Fig. 10. Case II: Snapshots of the experimental setup during manipulation.

5.3. Case III

In the last case study, the corresponding XYZ position of the end effector, XY position of the end of the 5th arm and constant joint space configuration $q_d = \{0, \pi/6, 0, -\pi/2, 0, \pi/3, 0\}$ are considered as the tasks in the hierarchy. Figs. 13 and 14 show the same performance of the controller when the tasks are the same in the first and second priorities. Robot reaction in the task space to the external interactions is similar to the previous cases and the error converges to zero right after the interaction with the robot body. The last interaction interval, in this case, consists of two consecutive external interactions in two different positions and directions.

5.4. Discussion

Experimental results show that by using the proposed controller–observers along with the priority allocation method, system stability is guaranteed and the manipulation performance is enhanced remarkably. The method performance in various hybrid force–position control (*Case I*), hybrid position–orientation control (*Case II*) is considerable. In *Case I*, the results demonstrate that the controller–observer efficiency is not limited to the interaction phase and enhances the manipulation accuracy all over the experiment. Moreover, employing uncertain inertia and Coriolis/centrifugal matrices or even neglecting Coriolis/centrifugal force do not make the method performance unacceptable. This issue is proven by multiple experiments carried out in similar cases by the authors and is in accordance with the report in Sadeghian et al.

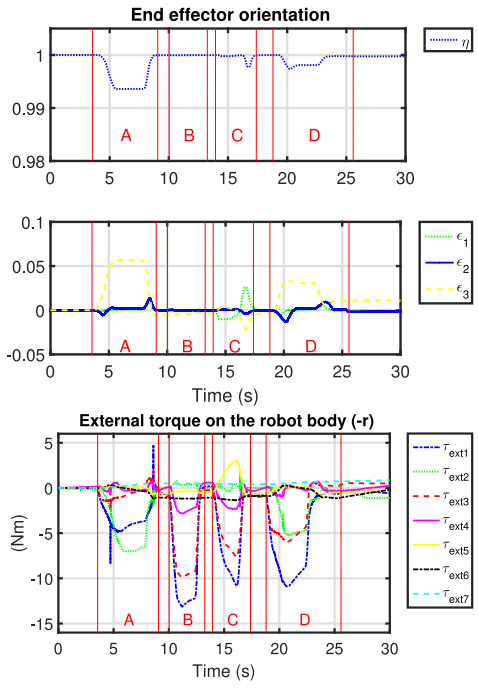

Fig. 11. Case II: Quaternion parameters (Top), External torques applied to the robot body (Bottom).

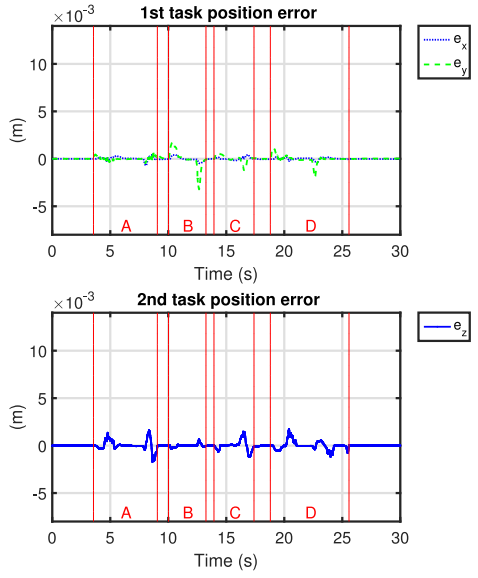

Fig. 12. Case II: First task position error (Top), Second task position error (Bottom).

(2014) for one position regulation task. All the model inaccuracies are computed in $\boldsymbol{\tau}_{ext}$ which is compensated in the control law.

During the experiments, external forces are applied to the different points on the robot body. The robot configuration changes compliantly when the interaction position is a bit far from the task accomplishment location (such as the one shown on the right side of Fig. 4). Interaction occurred in the intervals "A" and "D" in all the experiments are reporting this type of interactions. Considering joint space trajectory in Fig. 14, robot configuration is adopted compliantly to the external force in the null space of the higher priority tasks. Meanwhile, applying similar external force in the exact location of the defined tasks (during interaction intervals "B" and "C") does not change the robot configuration and causes a bigger external torque on the robot body which the proposed controller method is robust to that. Similar

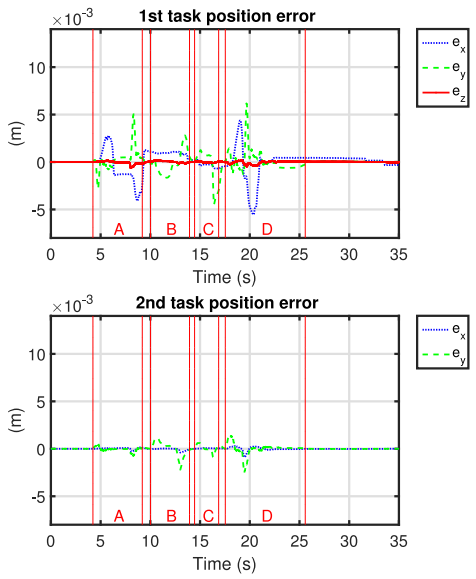

Fig. 13. Case III: First task position error (Top), Second task position error (Bottom).

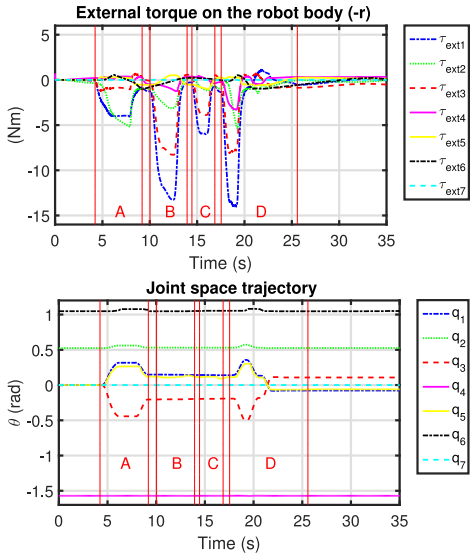

Fig. 14. Case III: External torques applied to the robot body (Top), Joint space trajectory (Bottom).

behavior was seen for robot joint space trajectory as the last task in other cases. Hence, we can conclude that all the intentions of the method for facilitating accurate and friendly accomplishment of various complex tasks at different priority level are met in the experiments.

It is noteworthy to consider that the control torque and the exchanged force during the physical interaction may increase significantly if the amount of the external force exceeds an acceptable limit which depends on the robot structure, tasks, *etc*.. A solution for this problem is to suspend the main manipulation tasks to show a compliance behavior through all degrees of freedom. In this situation, by replacing $\boldsymbol{Z}_{r-1}$ with $(n \times n)$ identity matrix in (26) and other equations along with omitting other tasks from (19), joint space impedance control can be obtained.

6. Conclusion

In this work, a novel controller–observer was proposed to accomplish various tasks at different priority levels. To this end, a new priority assignment scheme was investigated for priority allocation. The controller

guarantees accurate execution of multiple tasks besides compliant behavior in the null space during the interaction on the robot body. The proposed observer estimates the external interaction torques without using torque sensor and redundant degrees of freedom are exploited to realize a compliant behavior during the interaction. By using the proposed method, the disturbance effect in the main tasks is reduced significantly and in the case of no accidental interaction, the main task performance is enhanced considerably. Consequently, the robot can be utilized safely for accurate manipulation in human environments. Stability analysis of the system including force, position and orientation tasks control at different priority levels is given. The stability analysis scheme is in general form and covers various combinations of the tasks. Finally, the analytical analysis are confirmed by implementing the method in different cases on a 7DOF robot arm.

Conflict of interest

None declared.

Appendix A

For solving (21) and computing $\boldsymbol{r}(t)$ during empirical implementation with sampling time δt, trapezoidal rule is employed. Trapezoidal rule is a closed integration formula. In this method

$$\int_0^a f(\sigma)d\sigma \approx \frac{f(0)+2\Sigma_{i=1}^{i=n-1}f(\sigma_i)+f(a)}{2}\delta\sigma, \tag{A.1}$$

where $\delta\sigma = \frac{a-0}{n}$. By increasing n, $\delta\sigma$ approaches zero and this approximation is almost accurate (Chapra, 2004). Considering

$$\begin{aligned}&\int_0^t (\boldsymbol{\tau}+\boldsymbol{C}^T\dot{\boldsymbol{q}}-\boldsymbol{g}-\boldsymbol{J}_f^T\boldsymbol{f}_f+\boldsymbol{r}(\sigma))d\sigma = \\ &((\boldsymbol{\tau}(t)+\boldsymbol{C}(t)^T\dot{\boldsymbol{q}}(t)-\boldsymbol{g}(t)-\boldsymbol{J}(t)_f^T\boldsymbol{f}_f(t)+\boldsymbol{r}(t))+2\Sigma_{i=1}^{i=n-1}(\boldsymbol{\tau}(t-i\delta t)\\ &+\boldsymbol{C}(t-i\delta t)^T\dot{\boldsymbol{q}}(t-i\delta t)-\boldsymbol{g}(t-i\delta t)-\boldsymbol{J}_f^T(t-i\delta t)\boldsymbol{f}_f(t-i\delta t)+\boldsymbol{r}(t-i\delta t))\\ &+(\boldsymbol{\tau}(0)+\boldsymbol{C}(0)^T\dot{\boldsymbol{q}}(0)-\boldsymbol{g}(0)-\boldsymbol{J}(0)_f^T\boldsymbol{f}_f(0)+\boldsymbol{r}(0)))\delta t/2\end{aligned} \tag{A.2}$$

in (21), $\boldsymbol{r}(t)$ can be realized as

$$\begin{aligned}\boldsymbol{r}(t) =&\boldsymbol{K}_{obs}\Big(\boldsymbol{p}(t)-\big((\boldsymbol{\tau}(t)+\boldsymbol{C}(t)^T\dot{\boldsymbol{q}}(t)-\boldsymbol{g}(t)-\boldsymbol{J}(t)_f^T\boldsymbol{f}_f(t))\\ &+2\Sigma_{i=1}^{i=n-1}(\boldsymbol{\tau}(t-i\delta t)+\boldsymbol{C}(t-i\delta t)^T\dot{\boldsymbol{q}}(t-i\delta t)-\boldsymbol{g}(t-i\delta t)\\ &-\boldsymbol{J}_f^T(t-i\delta t)\boldsymbol{f}_f(t-i\delta t)+\boldsymbol{r}(t-i\delta t))+(\boldsymbol{\tau}(0)+\boldsymbol{C}(0)^T\dot{\boldsymbol{q}}(0)-\boldsymbol{g}(0)\\ &-\boldsymbol{J}(0)_f^T\boldsymbol{f}_f(0)+\boldsymbol{r}(0))\big)\delta t\Big)/(2+\boldsymbol{K}_{obs}\delta t).\end{aligned} \tag{A.3}$$

It is noteworthy to mention that the $\boldsymbol{r}(t)$ given by this equation is accurate according to the small time step of the system. By employing (A.3) one can obtain

$$\begin{aligned}\frac{\boldsymbol{r}(t)-\boldsymbol{r}(t-\delta t)}{\delta t} =&(\frac{\boldsymbol{K}_{obs}}{\delta t})\Big(\boldsymbol{p}(t)-\boldsymbol{p}(t-\delta t)-\big((\boldsymbol{\tau}(t)+\boldsymbol{C}(t)^T\dot{\boldsymbol{q}}(t)-\boldsymbol{g}(t)\\ &-\boldsymbol{J}(t)_f^T\boldsymbol{f}_f(t))+(\boldsymbol{\tau}(t-\delta t)+\boldsymbol{C}(t-\delta t)^T\dot{\boldsymbol{q}}(t-\delta t)-\boldsymbol{g}(t-\delta t)\\ &-\boldsymbol{J}_f^T(t-\delta t)\boldsymbol{f}_f(t-\delta t)+2\boldsymbol{r}(t-\delta t))\big)\delta t\Big)/(2+\boldsymbol{K}_{obs}\delta t).\end{aligned} \tag{A.4}$$

When $\delta t \longrightarrow 0$,

$$\begin{aligned}&\lim_{\delta t\longrightarrow 0}\frac{\boldsymbol{r}(t)-\boldsymbol{r}(t-\delta t)}{\delta t} = \dot{\boldsymbol{r}}\\ &=\boldsymbol{K}_{obs}(\dot{\boldsymbol{p}}(t)-(\boldsymbol{\tau}(t)+\boldsymbol{C}(t)^T\dot{\boldsymbol{q}}(t)-\boldsymbol{g}(t)-\boldsymbol{J}(t)_f^T\boldsymbol{f}_f(t)+\boldsymbol{r}(t))).\end{aligned} \tag{A.5}$$

and by considering (1), $\dot{\boldsymbol{p}} = \dot{\boldsymbol{M}}\dot{\boldsymbol{q}}+\boldsymbol{M}\ddot{\boldsymbol{q}}$, and $\dot{\boldsymbol{M}} = \boldsymbol{C}+\boldsymbol{C}^T$, ends to (22).

Appendix B. Supplementary data

Supplementary material related to this article can be found online at https://doi.org/10.1016/j.conengprac.2019.01.003.

References

Ajoudani, A., Tsagarakis, N. G., & Bicchi, A. (2011). Tele-impedance: Preliminary results on measuring and replicating human arm impedance in tele operated robots. In *2011 IEEE international conference on robotics and biomimetics* (pp. 216–222).

Bouyarmane, K., & Kheddar, A. (2011). Using a multi-objective controller to synthesize simulated humanoid robot motion with changing contact configurations. In *2011 IEEE/RSJ international conference on intelligent robots and systems* (pp. 4414–4419).

Caccavale, F., Chiaverini, S., & Siciliano, B. (1997). Second-order kinematic control of robot manipulators with jacobian damped least-squares inverse: theory and experiments. *IEEE/ASME Transactions on Mechatronics*, *2*(3), 188–194.

Caccavale, F., Natale, C., Siciliano, B., & Villani, L. (1998). Resolved-acceleration control of robot manipulators: A critical review with experiments. *Robotica*, *16*(05), 565–573.

Chang, P. (1987). A closed-form solution for inverse kinematics of robot manipulators with redundancy.

Chapra, S. C. (2004). *Applied numerical methods with MATLAB for engineering and science with engineering subscription card* (McGraw-Hill International edition). McGraw-Hill Higher Education.

Collette, C., Micaelli, A., Andriot, C., & Lemerle, P. (2007). Dynamic balance control of humanoids for multiple grasps and non coplanar frictional contacts. In *2007 7th IEEE-RAS international conference on humanoid robots* (pp. 81–88).

Corteso, R., & Dominici, M. (2017). Robot force control on a beating heart. *IEEE/ASME Transactions on Mechatronics*, *22*(4), 1736–1743.

De Luca, A., Ferri, M., Oriolo, G., & Giordano, P. (2008). Visual servoing with exploitation of redundancy: An experimental study. In *Robotics and automation, 2008. ICRA 2008. IEEE international conference on* (pp. 3231–3237). IEEE.

De Luca, A., & Mattone, R. (2005). Sensorless robot collision detection and hybrid force/motion control. In *Robotics and automation, 2005. ICRA 2005. Proceedings of the 2005 IEEE international conference on* (pp. 999–1004). IEEE.

De Luca, A., & Oriolo, G. (1997). Nonholonomic behavior in redundant robots under kinematic control. *IEEE Transactions on Robotics & Automation*, *13*(5), 776–782.

Flacco, F., & De Luca, A. (2014). A reverse priority approach to multi-task control of redundant robots. In *Intelligent robots and systems (IROS 2014), 2014 IEEE/RSJ international conference on* (pp. 2421–2427). IEEE.

Flacco, F., De Luca, A., & Khatib, O. (2012). Prioritized multi-task motion control of redundant robots under hard joint constraints. In *Intelligent robots and systems (IROS), 2012 IEEE/RSJ international conference on* (pp. 3970–3977). IEEE.

Hsu, P., Mauser, J., & Sastry, S. (1989). Dynamic control of redundant manipulators. *Journal of Robotic Systems*, *6*(2), 133–148.

Iggidr, B., Kalitine, A., & Outbib, R. (1996). Semidefinite lyapunov functions stability and stabilization. *Mathematics of Control, Signals & Systems*, *9*(2), 95–106.

Jin, L., & Li, S. (2018). Distributed task allocation of multiple robots: A control perspective. *IEEE Transactions on Systems, Man, & Cybernetics: Systems*, *48*(5), 693–701.

Jung, Seul, Hsia, T. C., & Bonitz, R. G. (2004). Force tracking impedance control of robot manipulators under unknown environment. *IEEE Transactions on Control Systems Technology*, *12*(3), 474–483.

Kesner, S. B., & Howe, R. D. (2011). Force control of flexible catheter robots for beating heart surgery. In *2011 IEEE international conference on robotics and automation* (pp. 1589–1594).

Khalil, H. K., & Grizzle, JW. (1996). *Nonlinear systems, volume 3*. Prentice hall New Jersey.

Khatib, O. (1987). A unified approach for motion and force control of robot manipulators: The operational space formulation. *IEEE Journal on Robotics & Automation*, *3*(1), 43–53.

Khatib, O. (1995). Inertial properties in robotic manipulation: An object-level framework. *The International Journal of Robotics Research*, *14*(1), 19–36.

Khatib, O., & Chung, S. Y. (2014). Suprapeds: Humanoid contact-supported locomotion for 3d unstructured environments. In *2014 IEEE international conference on robotics and automation (ICRA)* (pp. 2319–2325).

Khatib, M., Khudir, K. A., & De Luca, A. (2017). Visual coordination task for human–robot collaboration. In *2017 IEEE/RSJ international conference on intelligent robots and systems (IROS)* (pp. 3762–3768).

Liu, M., Tan, Y., & Padois, V. (2016). Generalized hierarchical control. *Autonomous Robots*, *40*(1), 17–31.

Mashayekhi, A., Behbahani, S., Ficuciello, F., & Siciliano, B. (2018). Analytical stability criterion in haptic rendering: The role of damping. *IEEE/ASME Transactions on Mechatronics*, *23*(2), 596–603.

Mistry, M., Nakanishi, J., & Schaal, S. (2007). Task space control with prioritization for balance and locomotion. In *Intelligent robots and systems, 2007. IROS 2007. IEEE/RSJ international conference on* (pp. 331–338). IEEE.

Nakanishi, J., Cory, R., Mistry, M., Peters, J., & Schaal, S. (2008). Operational space control: A theoretical and empirical comparison. *International Journal of Robotics Research*, *27*(6), 737–757.

Navkar, N. V., Deng, Z., Shah, D. J., Bekris, K. E., & Tsekos, N. V. (2012). Visual and force-feedback guidance for robot-assisted interventions in the beating heart with real-time mri. In *2012 IEEE international conference on robotics and automation* (pp. 689–694).

Nicolis, D., Zanchettin, A. M., & Rocco, P. (2016). Constraint-based and sensorless force control with an application to a lightweight dual-arm robot. *IEEE Robotics & Automation Letters*, *1*(1), 340–347.

Oh, Y., Chung, W., & Youm, Y. (1998). Extended impedance control of redundant manipulators based on weighted decomposition of joint space. *Journal of Robotic Systems*, *15*(5), 231–258.

Ott, C. (2008). *Cartesian Impedance Control of Redundant and Flexible-Joint Robots*. In *Springer Tracts in Advanced Robotics*, Springer Berlin Heidelberg.

Ott, C., Dietrich, A., & Albu-Schäffer, A. (2015). Prioritized multi-task compliance control of redundant manipulators. *Automatica*, *53*, 416–423.

Park, J., & Khatib, O. (2005). Multi-link multi-contact force control for manipulators. In *Robotics and automation, 2005. ICRA 2005. Proceedings of the 2005 IEEE international conference on* (pp. 3613–3618). IEEE.

Polverini, M. P., Rossi, R., Morandi, G., Bascetta, L., Zanchettin, A. M., & Rocco, P. (2016). Performance improvement of implicit integral robot force control through constraint-based optimization. In *2016 IEEE/RSJ international conference on intelligent robots and systems (IROS)* (pp. 3368–3373).

Sadeghian, H., Villani, L., Kamranian, Z., & Karami, A. (2015). Visual servoing with safe interaction using image moments. In *Intelligent robots and systems (IROS), 2015 IEEE/RSJ international conference on* (pp. 5479–5485).

Sadeghian, H., Villani, L., Keshmiri, M., & Siciliano, B. (2013). Dynamic multi-priority control in redundant robotic systems. *Robotica*, *31*(07), 1155–1167.

Sadeghian, H., Villani, L., Keshmiri, M., & Siciliano, B. (2014). Task-space control of robot manipulators with null-space compliance. *IEEE Transactions on Robotics*, *30*(2), 493–506.

Sadeghian, Hamid, Zokaei, Fatemeh, & Jazi, Shahram Hadian (2018). Constrained kinematic control in minimally invasive robotic surgery subject to remote center of motion constraint. *Journal of Intelligent and Robotic Systems*, 1–13.

Sato, F., Nishii, T., Takahashi, J., Yoshida, Y., Mitsuhashi, M., & Nenchev, D. (2011). Experimental evaluation of a trajectory/force tracking controller for a humanoid robot cleaning a vertical surface. In *2011 IEEE/RSJ international conference on intelligent robots and systems* (pp. 3179–3184).

Sentis, L., Park, J., & Khatib, O. (2010). Compliant control of multicontact and center-of-mass behaviors in humanoid robots. *IEEE Transactions on Robotics*, *26*(3), 483–501.

Siciliano, B., Sciavicco, L., & Villani, L. (2010). *Robotics : modelling, planning and control*. In *Advanced Textbooks in Control and Signal Processing*, London: Springer.

Siciliano, B., & Slotine, J. E. (1991). A general framework for managing multiple tasks in highly redundant robotic systems. In *Advanced robotics, 1991.'Robots in unstructured environments', 91 ICAR. Fifth international conference on* (pp. 1211–1216). IEEE.

Winkler, A., & Such, J. (2013). Force controlled contour following on unknown objects with an industrial robot. In *2013 IEEE international symposium on robotic and sensors environments (ROSE)* (pp. 208–213).

Zemiti, N., Morel, G., Ortmaier, T., & Bonnet, N. (2007). Mechatronic design of a new robot for force control in minimally invasive surgery. *IEEE/ASME Transactions on Mechatronics*, *12*(2), 143–153.